# Isolated Pt Atoms Stabilized by Ga₂O₃ Clusters Confined in ZSM-5 for Nonoxidative Activation of Ethane

Xiaomeng Dou,◆ Kailang Li,◆ Kun Zhang,◆ Chaofeng Zhu, Debora M. Meira, Yang Song, Peng He,* Liang Zhang,* and Lichen Liu*

Read Online

ACCESS | Metrics & More | Article Recommendations | Supporting Information

**ABSTRACT:** Selective activation of light alkanes is an essential reaction in the petrochemical industry for producing commodity chemicals, such as light olefins and aromatics. Because of the much higher intrinsic activities of noble metals in comparison to non-noble metals, it is desirable to employ solid catalysts with low noble metal loadings to reduce the cost of catalysts. Herein, we report the introduction of a tiny amount of Pt (at levels of hundreds of ppm) as a promoter of the Ga₂O₃ clusters encapsulated in ZSM-5 zeolite, which leads to ~20-fold improvement in the activity for ethane dehydrogenation reaction. A combination of experimental and theoretical studies shows that the isolated Pt atoms stabilized by small Ga₂O₃ clusters are the active sites for activating the inert C−H bonds in ethane. The synergy of atomically dispersed Pt and Ga₂O₃ clusters confined in the 10MR channels of ZSM-5 can serve as a bifunctional catalyst for the direct ethane−benzene coupling reaction for the production of ethylbenzene, surpassing the performances of the counterpart catalysts made with PtGa nanoclusters and nanoparticles.

**KEYWORDS:** *platinum, single atoms, gallium oxide, ZSM-5, ethane dehydrogenation, ethane−benzene coupling*
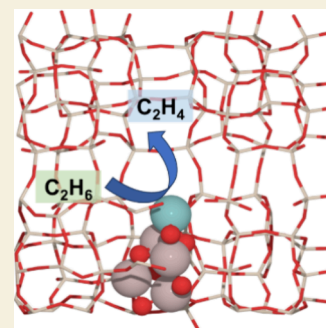
## INTRODUCTION

The abundant supply of light alkanes from the shale gas can serve as a substitute for petroleum in the chemical industry for the production of commodity chemicals such as light olefins (e.g., ethylene and propylene) and aromatics (e.g., benzene, toluene, xylenes, and styrene).[1,2] In particular, the selective conversion of ethane into olefins and aromatics is of great interest to the chemical industry because of their enormous global demands.[3] Currently, the principal utilization strategy for ethane is the steam cracking process for ethylene production.[4] Considering the high reaction temperature (>800 °C) required for the steam cracking process, it is desirable to develop efficient catalytic processes for converting ethane into ethylene or aromatics with low carbon emissions.[5]

Because of the inert nature of the C−H bonds in ethane, it usually requires the use of noble metals as the catalyst's functional component (e.g., Pt) and high reaction temperatures (e.g., > 600 °C) to achieve sufficient reaction rates under nonoxidative conditions.[6,7] Indeed, various types of Pt-based supported metal catalysts have been developed to activate ethane, among which the Pt species primarily exist as bimetallic or multimetallic nanoparticles (Figure 1a).[8−13] However, for catalytic processes aiming at nonoxidative ethane conversion into light olefins and aromatics, the high cost of the noble metal catalysts and their poor stability under high-temperature conditions and during consecutive reaction−regeneration cycles hinder their commercialization.

One practical strategy to promote the utilization efficiency of noble metals is to substitute conventional metal nanoparticles with atomically dispersed metal species, as demonstrated with single-atom alloy catalysts and atomically dispersed species on oxides.[14,15] However, if the noble metal active sites are supported on open-surface carriers (e.g., SiO₂ and Al₂O₃, as illustrated in Figure 1b), then avoiding the sintering issues is challenging under harsh reaction conditions.[16−19] To improve the stability of highly dispersed noble metal species, an effective approach is to encapsulate the tiny metal species into the micropores of zeolites, whose rigid framework will impose confinement effects on the metal species to limit their mobility under harsh reaction conditions.[20−23] This strategy has been practiced with zeolite-encapsulated subnanometer metal clusters (Figure 1c), which exhibit remarkably high stability for the dehydrogenation of light alkanes.[24−27] When translating this concept to stabilizing atomically dispersed noble metal species, the mismatch between the pore dimension and the size of the atomically dispersed metal species leads to the gradual sintering of metal atoms into small clusters and catalyst deactivation.[28]

In this work, we have attempted to tackle the above-mentioned stability issue by preparing a zeolite-encapsulated PtGa catalyst in which isolated Pt atoms are stabilized by GaOₓ
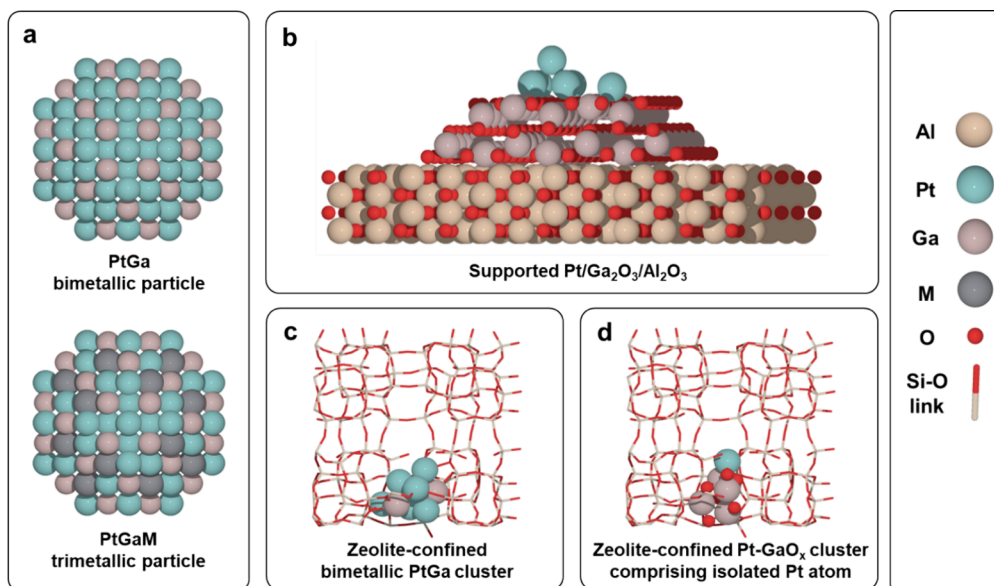
**Figure 1.** Illustration of the structural features of typical Pt-based catalysts for dehydrogenation of light alkanes. In this figure, we take the combination of Pt and Ga as the main active component as an exemplary description. (a) Bimetallic and trimetallic Pt-based nanoparticles. The Pt atoms are segregated by the Ga or a third metal, resulting in the formation of single-atom sites in the bimetallic and trimetallic nanoparticles. (b) Combination of subnanometer Pt sites (single Pt atoms or clusters) and $Ga_2O_3$ nanoparticles supported on $Al_2O_3$. (c) Zeolite-confined subnanometer PtGa clusters made with metallic Pt species and reduced $GaO_x$ or metallic Ga species. (d) Pt-$GaO_x$ sites made with a single Pt atom and a $GaO_x$ cluster. The Pt-$GaO_x$ clusters are confined in the microporous channels of the zeolite.

clusters confined in the 10MR channels of ZSM-5 zeolite (Figure 1d). The ensemble of a single Pt atom and a $GaO_x$ cluster matches well with the micropores of the ZSM-5 zeolite, resulting in a strong confinement effect between the Pt-$GaO_x$ cluster and the zeolite framework. Furthermore, we have revealed that the $GaO_x$ nanoclusters with an average particle size of ~1 nm promoted with single Pt atoms can deliver better specific activity for activating C−H bonds in ethane than other reported supported Pt catalysts.

## RESULTS AND DISCUSSION

### Synthesis and Characterization of Ga-ZSM5 Materials

Ga-modified ZSM-5 zeolites have been reported as non-noble metal catalysts for activating light alkanes.[29] To achieve a good dispersion of Ga species within the ZSM-5 zeolite crystallites, we have prepared a series of Ga-ZSM5 samples with good crystallinity via a one-pot synthesis approach (see XRD patterns in Figure S1). The Si/Al of the final Ga-ZSM5 materials is fixed to ~55 for all the Ga-ZSM5 samples, and the Ga loading is tuned by modifying the amount of the Ga precursor in the synthesis mixture (see synthesis details and composition analysis results in Tables S1 and S2). Figure S2 shows that the 3Ga-ZSM5 sample with a Ga loading of ~3.0 wt % gives the highest normalized activity for EDH among the Ga-ZSM5 samples. Electron microscopy characterization results show that the particle size of the $GaO_x$ species in the ZSM-5 zeolite is dependent on the Ga loading (Figures S3−S6). When the Ga loading increases from 0.5 to 4.8 wt %, the average particle size of $GaO_x$ species gradually increases from <1 to ~2 nm (Figure S7). Some literature works propose that atomically dispersed Ga species or binuclear Ga species formed at the Brønsted acid sites of ZSM-5 are responsible for alkane dehydrogenation reaction.[30−33] One major difference between the reported works and our system is that the Ga-ZSM5 samples prepared in our work contain alkali metal (i.e., K+),

which compensates for the Brønsted acid sites, resulting in the formation of $GaO_x$ clusters/nanoparticles encapsulated inside the ZSM-5 crystallites instead of the atomically dispersed Ga species anchored at the Brønsted acid sites. We have prepared a series of K-free Ga-ZSM5 samples by one-pot synthesis for comparison. As indicated by the HAADF-STEM images (Figures S8−S11), the dispersion of the Ga species within the ZSM-5 zeolite crystallites is indeed improved in the absence of K+. However, the catalytic results of the K-free Ga-ZSM5 samples show that the absence of K+ will not promote the activity of the Ga species (Figure S12), inferring that the K-promoted Ga-ZSM5 catalyst derived from a one-pot synthesis can also be an active catalyst for EDH.

However, from a practical point of view, the Ga-ZSM5 catalysts give limited space-time yields of ethylene due to the relatively low intrinsic activities of Ga species for C−H activation. Recent studies show that, by the introduction of a small number of noble metals (e.g., Ir and Pt) in the oxide-supported $GaO_x$ catalysts, considerable improvements in activities for propane dehydrogenation reaction can be achieved, suggesting the remarkable synergy of noble metals and $GaO_x$ particles.[15,34] In light of the prior works, we hypothesize that if the Pt and $GaO_x$ species are both encapsulated in a zeolite matrix, the resultant Pt-$GaO_x$ species could be stabilized by the rigid zeolite framework, resulting in highly active bimetallic sites for the selective transformation of light alkanes with long-term stability.

### Synthesis and Characterization of PtGa-ZSM5 Materials

To ensure the encapsulation of subnanometer Pt species in the ZSM-5 structure, the Pt-containing zeolite materials are also synthesized by the one-pot method (Figure S13). The Ga loading is fixed at ~3.0 wt % because of the good catalytic performance of 3Ga-ZSM5 for EDH, while the Pt loading is tuned in the range of 0.004−0.4 wt %, giving the formation of a series of $y$Pt-3Ga-ZSM5 samples ($y$ refers to the loading of Pt).
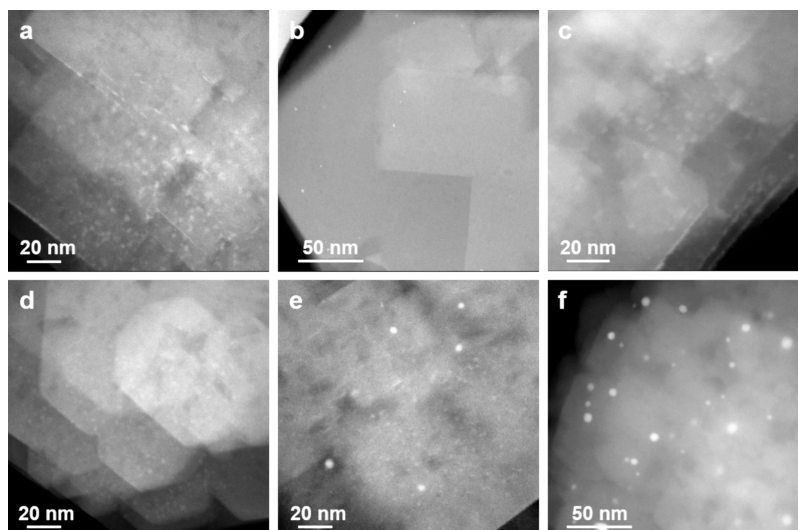
**Figure 2.** HAADF-STEM images of metal-zeolite materials with different compositions. (a) 3Ga-ZSM5, (b) 0.04Pt-ZSM5, (c) 0.011Pt-3Ga-ZSM5, (d) 0.04Pt-3Ga-ZSM5, (e) 0.15Pt-3Ga-ZSM5, and (f) 0.43Pt-3Ga-ZSM5 samples. In the 3Ga-ZSM5 sample, we can observe the presence of GaO$_x$ clusters within the ZSM-5 crystallites. In the 0.04Pt-ZSM5 sample, small Pt nanoparticles are observed. Regarding the 0.011Pt-3Ga-ZSM5 and 0.04Pt-3Ga-ZSM5 samples, they show a morphology similar to that of the 3Ga-ZSM5 sample because the Pt species predominantly exist as atomically dispersed species, which are not visible in these low-magnitude HAADF-STEM images. In the 0.15Pt-3Ga-ZSM5 and 0.43Pt-3Ga-ZSM5 samples, some Pt clusters and nanoparticles with high contrast (brightness in the HAADF-STEM images) are observed due to the high Pt loadings.
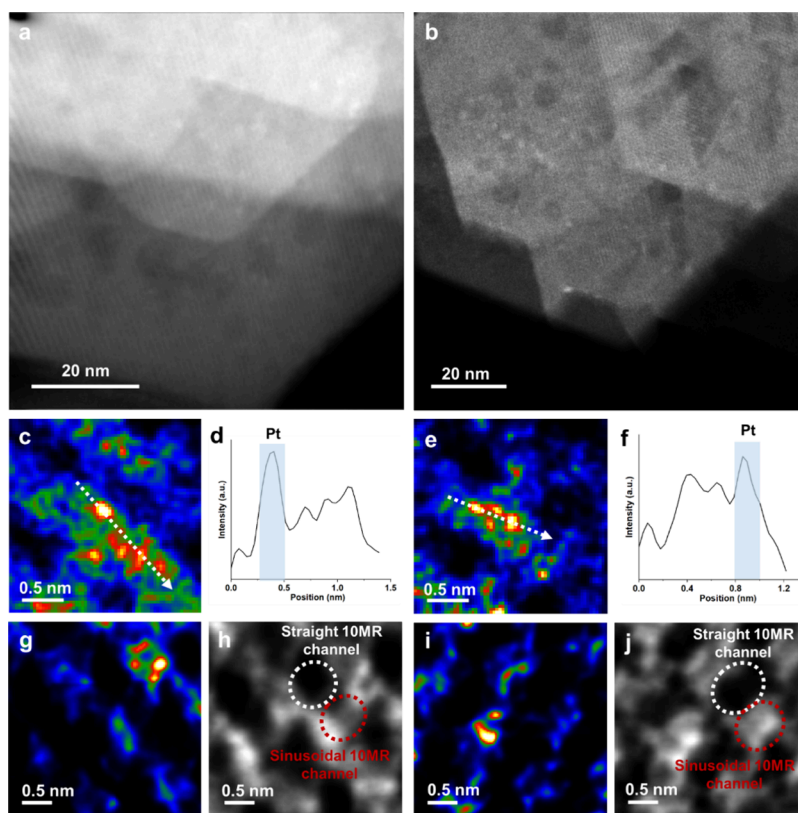


**Figure 3.** Characterization of the 0.04Pt-3Ga-ZSM5 sample by high-resolution electron microscopy. (a,b) Low-magnitude HAADF-STEM images of the 0.04Pt-3Ga-ZSM5 sample, showing the presence of GaO$_x$ clusters. Due to the low magnitude, the single Pt atoms are not visible in these images. (c,e) High-resolution HAADF-STEM images of Pt-GaO$_x$ clusters and (d,f) corresponding intensity profiles of the Pt-GaO$_x$ clusters. The baselines of the contrast profiles are influenced by the thickness of the zeolite support. Nevertheless, based on the working principle of the HAADF-STEM imaging technique, the positions of the single Pt atoms can be determined due to their much higher contrasts than the neighboring atoms (Ga or O atoms). (g–j) Representative HAADF-STEM and the paired iDPC-STEM images of the Pt-GaO$_x$ clusters in the 0.04Pt-3Ga-ZSM5 sample, which indicate their locations in the sinusoidal 10MR channels of the ZSM-5 zeolite. The sinusoidal and straight 10MR channels are marked in the iDPC-STEM images.
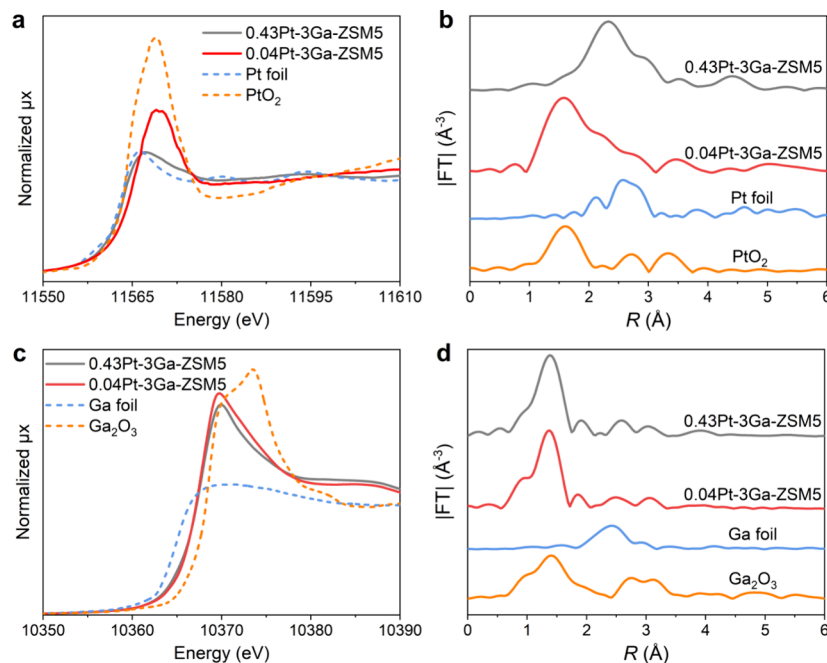
**Figure 4.** Characterization of PtGa-ZSM5 materials by X-ray absorption spectroscopy. Pt $L_3$-edge XANES (a) and EXAFS (b) spectra and references (Pt foil and $PtO_2$). Ga K-edge XANES (c) and EXAFS (d) spectra and references (Ga foil and $Ga_2O_3$).

**Table 1. Fit Results of the Pt L3-Edge and Ga K-Edge EXAFS Spectra**

| sample | edge | scattering pair | CN | R (Å) | $\sigma^2$ (Å$^2$) | $\Delta E_0$ (eV) | R factor |
|---|---|---|---|---|---|---|---|
| 0.04Pt-3Ga-ZSM5 | Pt | Pt—O | 3.79 ± 0.51 | 1.99 ± 0.01 | 0.001 ± 0.0025 | 8.90 ± 0.69 | 0.0065 |
| | Ga | Ga—O | 4.07 ± 0.35 | 1.78 ± 0.01 | 0.0044 ± 0.0011 | 1.50 ± 1.25 | 0.0047 |
| 0.43Pt-3Ga-ZSM5 | Pt | Pt—Ga | 6.59 ± 0.50 | 2.62 ± 0.03 | 0.0063 ± 0.002 | 2.28 ± 1.21 | 0.013 |
| | | Pt—Pt | 0.61 ± 0.23 | 2.78 ± 0.02 | 0.007 ± 0.003 | 2.28 ± 1.21 | 0.013 |
| | Ga | Ga—O | 4.85 ± 0.53 | 1.81 ± 0.01 | 0.0052 ± 0.0013 | 1.67 ± 0.22 | 0.0043 |

In the Ga-ZSM5 sample, we observed the formation of $GaO_x$ nanoclusters within the ZSM-5 crystallites (Figure 2a). Regarding the Pt-ZSM5 sample, small Pt nanoparticles with particle sizes of 1–2 nm are observed (Figure 2b), and the formation of Pt nanoparticles instead of subnanometer Pt clusters should be related to the absence of reducible oxides as anchoring sites for subnanometer Pt species.[35]

When the Pt loading is ≤0.04 wt %, the PtGa-ZSM5 samples exhibit almost the same morphology as the Pt-free Ga-ZSM5 sample, and we can barely observe Pt clusters/nanoparticles in the HAADF-STEM images (Figure 2c,d and Figures S14–S17), implying that the Pt species are probably atomically dispersed within the zeolite support. High-resolution HAADF-STEM images confirm the presence of atomically dispersed Pt species in the 0.04Pt-3Ga-ZSM5 sample, as indicated by the profiles of the HAADF-STEM images (Figure 3a–f). According to the paired HAADF-STEM and integrated differential phase contrast (iDPC-STEM) images shown in Figure 3g–j and Figure S18, a considerable amount of the Pt-modified $GaO_x$ nanoclusters is located in the sinusoidal channels of MFI zeolite.[36] A further increase in the Pt loading to 0.15 wt % will cause the formation of subnanometer Pt clusters and a few Pt nanoparticles (Figure 2e and Figure S19), as indicated by the bright particles in the HAADF-STEM images. When the Pt loading is further elevated to 0.4 wt %, a considerable number of PtGa bimetallic nanoparticles are formed (Figure 2f and Figure S20), according to the energy-dispersive spectroscopy (EDS) analysis (Figure S21). The

formation of PtGa bimetallic nanoparticles is likely caused by the reduction of $GaO_x$ species promoted by Pt nanoparticles.[37,38] These results clearly show that the size distributions of the Pt species are closely related to the Pt loadings, which should be maintained at ≤0.15 wt % to ensure the formation of subnanometer Pt species in Ga-ZSM5.

We further employed spectroscopic characterization techniques to probe the dispersion of Pt species within the PtGa-ZSM5 samples. As displayed in Figure 4a, the in situ X-ray absorption near-edge spectroscopy (XANES) results show that the electronic properties of the Pt species are dependent on the Pt loading. In the 0.43Pt-3Ga-ZSM5 sample reduced by $H_2$ at 600 °C, Pt species mainly exist as metallic Pt species, while in the case of the reduced 0.04Pt-3Ga-ZSM5 sample, the Pt species exist as positively charged $Pt^{\delta+}$ species, probably in the form of $Pt^{2+}$ species, according to the analysis of the white-line intensity of the XANES spectra.[39–41] In the 0.43Pt-3Ga-ZSM5 sample, both Pt—Pt and Pt—Ga bonding is observed in the Pt $L_3$-edge EXAFS spectra, corresponding to the presence of PtGa alloyed nanoparticles (Figure 4b, Figures S22–S24, and Table 1). In the case of the 0.04Pt-3Ga-ZSM5 sample, only the first-shell Pt—O bonding is observed instead of Pt—Pt or Pt—Ga bonding, implying the presence of isolated $Pt^{\delta+}$ species, which is consistent with the electron microscopy images.

According to the in situ XANES spectra, the Ga species in the two PtGa-ZSM5 samples should predominantly exist in the form of $Ga^{3+}$ species because the XANES spectra almost resemble that of the $Ga_2O_3$ standard sample (Figure 4c). The
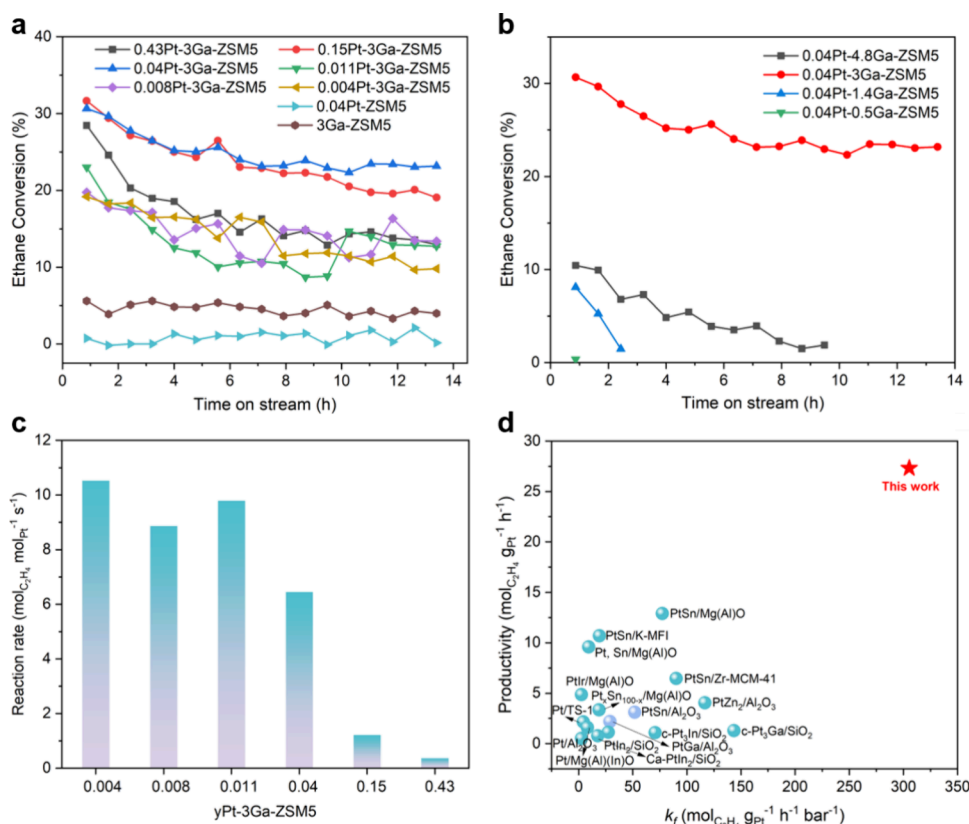
**Figure 5.** Catalytic tests of metal-zeolite catalysts for EDH. (a) Catalytic performances of Pt-ZSM5, Ga-ZSM5, and PtGa-ZSM5 catalysts with different Pt contents for EDH. (b) Catalytic performances of 0.04Pt-$x$Ga-ZSM5 catalysts with different Ga loadings. Reaction conditions: 600 °C, 200 mg of the catalyst, $C_2H_6/N_2$ with a ratio of 1/9 and a total flow of 50 mL/min as the feed gas. (c) Initial specific activities of Pt-ZSM5, Ga-ZSM5, and PtGa-ZSM5 catalysts for EDH. These results were obtained under the kinetic regime and normalized to the total number of Pt atoms in the sample. The conversion of $C_2H_6$ is controlled to be in the kinetic regime (ethane conversions below 15%) by varying the weight hourly space velocity. It should be noted that, under our reaction conditions, the thermodynamic equilibrium conversion of ethane is 44.2% by assuring that ethylene is the only product. (d) Specific forward reaction rate $k_f$ and productivity of 0.04Pt-3Ga-ZSM5 and other catalysts reported in the literature for EDH at 600−660 °C. The specific forward reaction rates of different catalysts were calculated based on the catalytic results presented in the literature works. Detailed information about the catalysts is summarized in Table S3.

presence of $Ga^{3+}$ species in the PtGa-ZSM5 samples is further confirmed by the quasi in situ XPS characterization (Figure S25), in which the sample is transferred to the analysis chamber without exposure to air after reduction treatment by $H_2$. Only the first-shell Ga−O bonding is observed in the EXAFS spectra, while the Ga−O−Ga bonding is barely observed, which should be associated with the low sensitivity of EXAFS for detecting the long-range bonding the $Ga_2O_3$ clusters with particle sizes below 1.5 nm (Figure 4d and Table 1).[42−44] Though we have observed the formation of bimetallic PtGa nanoparticles in the 0.43Pt-3Ga-ZSM5 sample, a vast majority of the Ga species are not in contact with Pt species, resulting in the absence of Ga−Pt bonding in the Ga K-edge EXAFS spectra. The predominant contribution of $Ga_2O_3$ in the PtGa-ZSM5 samples is supported by the absence of reduction peaks in the temperature-programmed reduction (TPR) profiles due to the negligible reducibility of $Ga_2O_3$ nanoparticles (Figure S26).

## Catalytic Results for Ethane Dehydrogenation Reaction

We employed EDH as the probe reaction to study the catalytic performances of the PtGa-ZSM5 catalysts with different compositions and structural features. Initially, we tested a series of 3Ga-ZSM5 catalysts promoted with different Pt loadings. As shown in Figure 5a, when testing under the same

conditions (feed composition, reaction temperature, weight hourly space velocity, etc.), the ethane conversion greatly depends on the composition of the solid catalyst. For monometallic Pt-ZSM5 and Ga-ZSM5 samples, low activities are obtained. Interestingly, even after the addition of ~80 ppm Pt, the initial ethane conversion can be promoted by nearly four times, increasing from ~5 to ~20%. When the Pt loading is further elevated to ~400 ppm (i.e., the 0.04Pt-3Ga-ZSM5 sample), a high initial conversion and good stability can be achieved. Interestingly, a further increase in the Pt loading to 0.15 wt % will lead to a catalyst with similar initial ethane conversion but a faster deactivation rate. This tendency is more marked in the 0.43Pt-3Ga-ZSM5 sample, indicating that the stability of the PtGa-ZSM5 catalysts against deactivation under the EDH conditions also depends on the Pt loading. The kinetic measurements on the reaction order of ethane in the EDH are also in line with the activity results, in which we have observed different reaction orders of ethane in three metal-zeolite catalysts, implying that the nature of the active sites may vary with the Pt loading (Figure S27).[45,46]

As shown in Figure S28, at the initial stage, the relatively low selectivity to ethylene is caused by the coke deposition on the acid sites, which accounts for the production of side products (mainly in the form of aromatics). With the increase in the coke content, the selectivity to ethylene increases substantially.

It should be noted that after ~6 h, the catalyst reaches a relatively stable state for the ethane dehydrogenation reaction, which could be caused by the blocking of the acid sites by coke, as probed by Raman spectra of the spent catalysts (Figure S29).

We calculated the normalized mass activity of various PtGa-ZSM5 catalysts to figure out the intrinsic activity of different types of Pt species in various catalysts. As displayed in Figure 5c, a plateau of specific activity is observed when the Pt loading is ≤0.011 wt %, and the normalized activity gradually decreases with the Pt loadings above 0.011 wt %. By correlating the catalytic results and the structural characterizations of the PtGa-ZSM5 samples, we tentatively think that atomically dispersed Pt species formed in Ga-ZSM5 are the most efficient species for EDH, while monometallic Pt clusters, bimetallic PtGa clusters, or PtGa nanoparticles are less active. The comparison of the 0.04Pt-3Ga-ZSM5 sample with the reported catalysts made with Pt-based clusters/nanoparticles further confirms the superior performances of the atomically dispersed Pt species on $Ga_2O_3$ clusters in terms of the specific activity normalized to Pt mass and the specific forward reaction rates derived from thermodynamic calculations (see the calculation method in Supplementary Note 1 and the performance summary in Figure 5d and Table S3).[47] We would like to emphasize that the high specific activity obtained with the Pt−$Ga_2O_3$ sites is achieved under the condition of $H_2$-free in the EDH reaction feed, which is different from the catalytic behavior of the Pt-$GaO_x$ sites formed on $Al_2O_3$, in which the cofeeding of $H_2$ is necessary for achieving high activity in the propane dehydrogenation reaction.[18,34]

The above results demonstrate the sensitivity of the dispersion of Pt species in the Ga-ZSM5 catalyst for EDH. Considering that the size of $Ga_2O_3$ particles in the Ga-ZSM5 samples can be modulated by the Ga loading, we further study a series of PtGa-ZSM5 catalysts with the same Pt loading (0.04 wt %) but varied Ga loadings (0.5 to 4.8 wt %). As presented in Figures S30 and S31, morphological characterizations by the HAADF-STEM imaging technique show that, in the case of PtGa-ZSM5 samples with low Ga loadings (0.5 and 1.4 wt %), small $Ga_2O_3$ clusters are well-dispersed within ZSM-5 crystallites. Consequently, it is speculated that the probability of forming sufficient bimetallic Pt−$Ga_2O_3$ sites will be low due to the low densities of Pt and Ga sites across the ZSM-5 crystallites. In the case of the PtGa-ZSM5 sample with a Ga loading of 4.8 wt %, $Ga_2O_3$ nanoparticles of >1.5 nm are formed, which may exhibit different catalytic properties from the single Pt atoms supported on $Ga_2O_3$ nanoclusters, because the electronic properties of $Ga_2O_3$ particles can vary substantially with the particle size (Figure S32).[48,49]

As presented in Figure 5b and Figure S33, only the PtGa-ZSM5 catalyst with a Ga loading of 3.0 wt % shows high activity for EDH, while catalysts with lower or higher Ga loadings give poor performances. In addition, we have prepared several PtGa-ZSM5 catalysts with fixed Pt and Ga loadings but with varied Si/Al ratios (see compositions in Table S2). As shown in Figure S34, 0.04Pt-3Ga-ZSM5 with a Si/Al ratio of 56 (the characterizations of the PtGa-ZSM5 catalysts with different Si/Al ratios are shown in Figures S35−S39) exhibits the best performance. Though the 0.04Pt-3Ga-ZSM5 with a Si/Al ratio of 56 shows a relatively low selectivity to ethylene due to the side reactions on acid sites in ZSM-5, its selectivity can be promoted by increasing the prereduction temperature to 650 °C before the EDH test. In the long-term

stability test shown in Figure S40, after the induction period (~10 h) for blocking the undesired acid sites by coking, a high selectivity to ethylene can be obtained, accompanied by a slow deactivation rate at 600 °C. The electron microscopy characterizations suggest that the domain size of the $Ga_2O_3$ particles is also dependent on the Si/Al ratio. Considering the structural complexity of PtGa-ZSM5 catalysts with different Si/Al ratios (crystallinity of ZSM-5, spatial distribution of $Ga_2O_3$ and Pt species, and the particle size of $Ga_2O_3$), the structure−reactivity relationship for ethane dehydrogenation reaction is established on the PtGa-ZSM5 samples with a fixed Si/Al ratio, as will be shown later in this manuscript on studying the impact of the domain size of $Ga_2O_3$ species.

The high-temperature stability is a critical issue with supported single-atom catalysts, especially during consecutive oxidation−reduction treatments. As shown in Figure S41, the $Al_2O_3$-supported PtGa catalyst with similar Pt and Ga loadings to the 0.04Pt-3Ga-ZSM5 sample suffers severe sintering of Pt species into large nanoparticles after three consecutive oxidation−reduction treatments at 600 °C. By confining the Pt species inside the ZSM-5 crystallites, the high dispersion state of Pt species can be maintained after harsh treatments after the same aging treatment (Figure S42). We have also tested the stability of the 0.04Pt-3Ga-ZSM5 catalyst for consecutive reaction−regeneration cycles at 600 °C. As shown in Figures S43 and S44, both its catalytic performance and morphology are maintained after the cyclic tests. The above catalytic results demonstrate that by confining the bimetallic Pt−$Ga_2O_3$ sites made by single Pt atoms dispersed on $Ga_2O_3$ nanoclusters in ZSM-5 zeolite, both high activity and stability for the ethane dehydrogenation reaction can be achieved, demonstrating a new concept of designing atomically dispersed noble metal catalysts for reactions under harsh conditions.

## Mechanistic Study by Theoretical Calculations and Experiments

To gain further insight into the distinct catalytic properties of various PtGa-ZSM5 catalysts, we have constructed several computational models to study the performances of the representative active sites by DFT calculations (Figure S45). We first study the activation of ethane on a bimetallic PtGa(111) surface, in which two types of exposed Pt sites are modeled.[50] As shown in Figure 6a,b, on the Pt-rich PtGa(111) surface with a continuous $Pt_3$ ensemble (denoted as the PtGa(111)-$Pt_3$ site), low energy barriers for activation of ethane are obtained, but the consecutive dehydrogenation of ethylene is very likely to occur as implied by the low energy barrier of the activation of C−H bonds in ethylene. As a result, the overdehydrogenation of ethylene will induce the coke formation on PtGa(111)-$Pt_3$ sites and rapid catalyst deactivation. In the case of the PtGa-terminated PtGa(111) surface with an isolated Pt atom (denoted as the PtGa(111)-$Pt_1$ site), high activity and stability against coke deposition can be obtained. The catalytic results show that the 0.43Pt-3Ga-ZSM5 sample exhibits low normalized Pt mass activity in the EDH test, which could be caused by the low abundance of the PtGa(111)-$Pt_1$ site in the realistic catalyst.

In addition, several models made by gallium oxide clusters and a single Pt atom are constructed in MFI-type zeolite to understand the catalytic behavior of PtGa-ZSM5 catalysts (Figures S46−S51 and Tables S4−S9). The extra framework species are located in the sinusoidal channels according to the
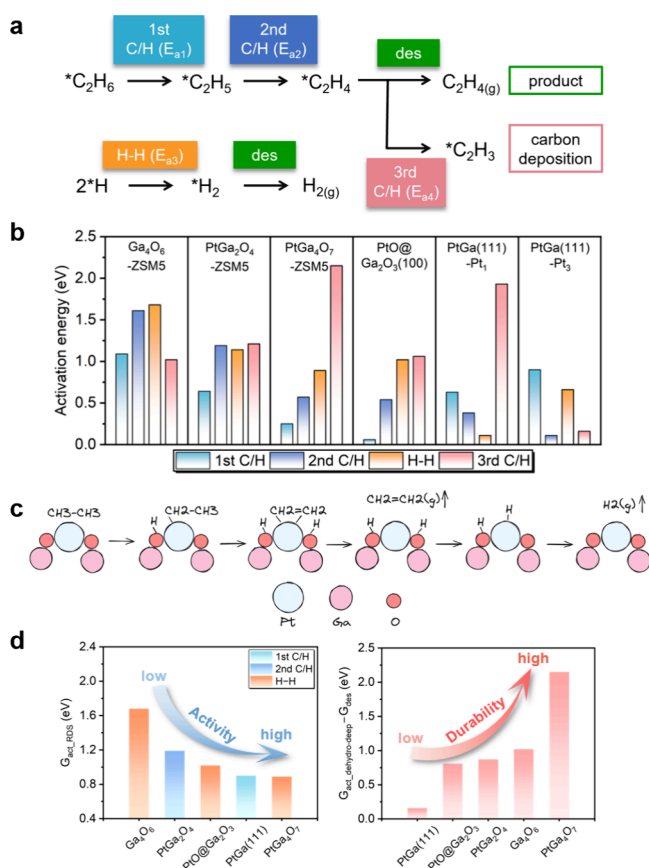
**Figure 6.** Theoretical studies on ethane dehydrogenation over PtGa-based catalysts. (a) Reaction mechanism for ethane dehydrogenation. (b) Activation energy for the elementary reaction steps during ethane dehydrogenation over different catalytic models. (c) Schematic diagram of the catalytic mechanism for ethane dehydrogenation over PtGa-ZSM5 catalysts. (d) Trend diagrams of the reaction activity and durability over different catalytic models.

HAADF-STEM and iDCP-STEM images (Figure 3). As shown in Figure 6b and Figure 6d, without the Pt promoter, the $Ga_4O_6$ cluster gives high energy barriers for activating C—H bonds in ethane, which is consistent with the low catalytic activities observed with the Ga-ZSM5 samples. After introduction of an isolated Pt(II) atom onto the $Ga_4O_6$ cluster, the $PtGa_4O_7$ structure (combination of PtO and $Ga_4O_6$) shows much lower energy barriers for cleavage of the C—H bonds in ethane. Furthermore, if the single-atom Pt promoter is located on a $Ga_2O_3$ cluster, the energy barrier for activating the C—H bonds will be considerably elevated, resulting in low catalytic activity. The insights derived from theoretical calculations are in line with our catalytic testing results, in which we have observed that the PtGa-ZSM5 sample with very small $Ga_2O_3$ nanoclusters gives low activities, while the PtGa-ZSM5 sample with $Ga_2O_3$ nanoclusters of ∼1 nm shows high activity for EDH. Nevertheless, the low activity of the 0.04Pt-4.8Ga-ZSM5 sample comprising $Ga_2O_3$ nanoparticles of >1.5 nm can be explained by the high energy barriers for the recombination of $H_2$ on the Pt-modified $Ga_2O_3(100)$ surface (the PtO@$Ga_2O_3$ model). This result can also explain the lower dependence of the 0.04Pt-3Ga-ZSM5 catalyst on $H_2$ partial pressure in EDH than the Pt-GaO$_x$ sites on the Pt−$Ga_2O_3$/$Al_2O_3$ catalyst, which relies on the cofeeding

of $H_2$ in the reaction feed for propane dehydrogenation reaction.[34]

We further conducted experiments to validate the conclusions drawn from theoretical calculations. The high capability of the Pt-promoted $Ga_2O_3$ cluster for ethane activation is confirmed by the temperature-programmed surface reaction (TPSR) profiles, in which the 0.04Pt-3Ga-ZSM5 sample starts to produce ethylene at 326 °C, while other catalysts require much higher temperatures to initiate the EDH process (Figure S52). The TPSR results match well with those from the isotopic study, in which we can observe higher exchange rates of C−H with $D_2$ on Pt-promoted $Ga_2O_3$ nanoclusters than on PtGa alloy nanoparticles (Figure S53).

With information obtained from theoretical and experimental approaches, we can now propose the reaction mechanism of EDH on the PtGa-ZSM5 catalyst (Figure 6c). The cleavage of the first C−H bond on $PtGa_4O_7$ clusters results in forming *$C_2H_5$ intermediate adsorbed on the Pt site and the Ga−OH species. After the cleavage of the second C−H bond, the $C_2H_4$ product will desorb from the active site, and the recombination of the *H species proceeds via the H-transfer from Ga−OH to the Pt site. Compared to the EDH on the $Ga_4O_6$ cluster and the Pt-modified $Ga_2O_3$ surface, the $H_2$ recombination step on the $PtGa_4O_7$ cluster can proceed with a lower energy barrier. The above-mentioned reaction mechanism has been verified by in situ IR experiments. As shown in Figure S54, an increase in the amount of Ga−OH species is observed after the adsorption of $C_2H_6$ on the 0.04Pt-3Ga-ZSM5 sample accompanied by the formation of $C_2H_4$ species on the catalyst surface, which is consistent with the occurrence of EDH and the formation of Ga−OH species suggested by the theoretical calculations. During the purging treatment with argon, the adsorbed hydrocarbon species are removed from the catalyst surface together with the desorption of $H_2$, resulting in the decrease in Ga−OH species.

The coke deposition caused by the overdehydrogenation of $C_2H_4$ on the active sites is another critical issue associated with the catalyst's stability in the reaction stream. As displayed in Figure 6b,d, the theoretical calculations show that the energy barrier for the cleavage of the C−H bond in $C_2H_4$ is lower on the Pt-modified $Ga_2O_3(100)$ surface (the Pt@$Ga_2O_3$ model with a barrier of 1.05 eV) than on the $PtGa_4O_7$ cluster (2.15 eV). Our control experiment with a reference Pt−$Ga_2O_3$/$Al_2O_3$ sample indeed shows a faster deactivation rate than the 0.04Pt-3Ga-ZSM5 sample for EDH under the same condition (Figure S55).

## Catalytic Results for Direct Coupling of Ethane and Benzene

The simultaneous presence of acid sites and metal sites in the PtGa-ZSM5 catalyst enables the possibility of a direct coupling reaction of ethane and benzene via the tandem ethane dehydrogenation and ethylene alkylation reaction on Pt−$Ga_2O_3$ sites and the Brønsted acid sites from the ZSM-5 zeolite, respectively (Figure 7a). As shown in Figure 7b−e, the 3Ga-ZSM5 sample gives very low ethane conversion and negligible benzene conversion, which could be associated with its low capability for the ethane dehydrogenation reaction. The 0.04Pt-3Ga-ZSM5 sample exhibits both good activity and good selectivity to ethylbenzene (close to 80%) in the direct ethane−benzene coupling reaction. Further increases in the Pt loading will not cause a further increase in yields of aromatics, which could be ascribed to the lower alkylation activity of the
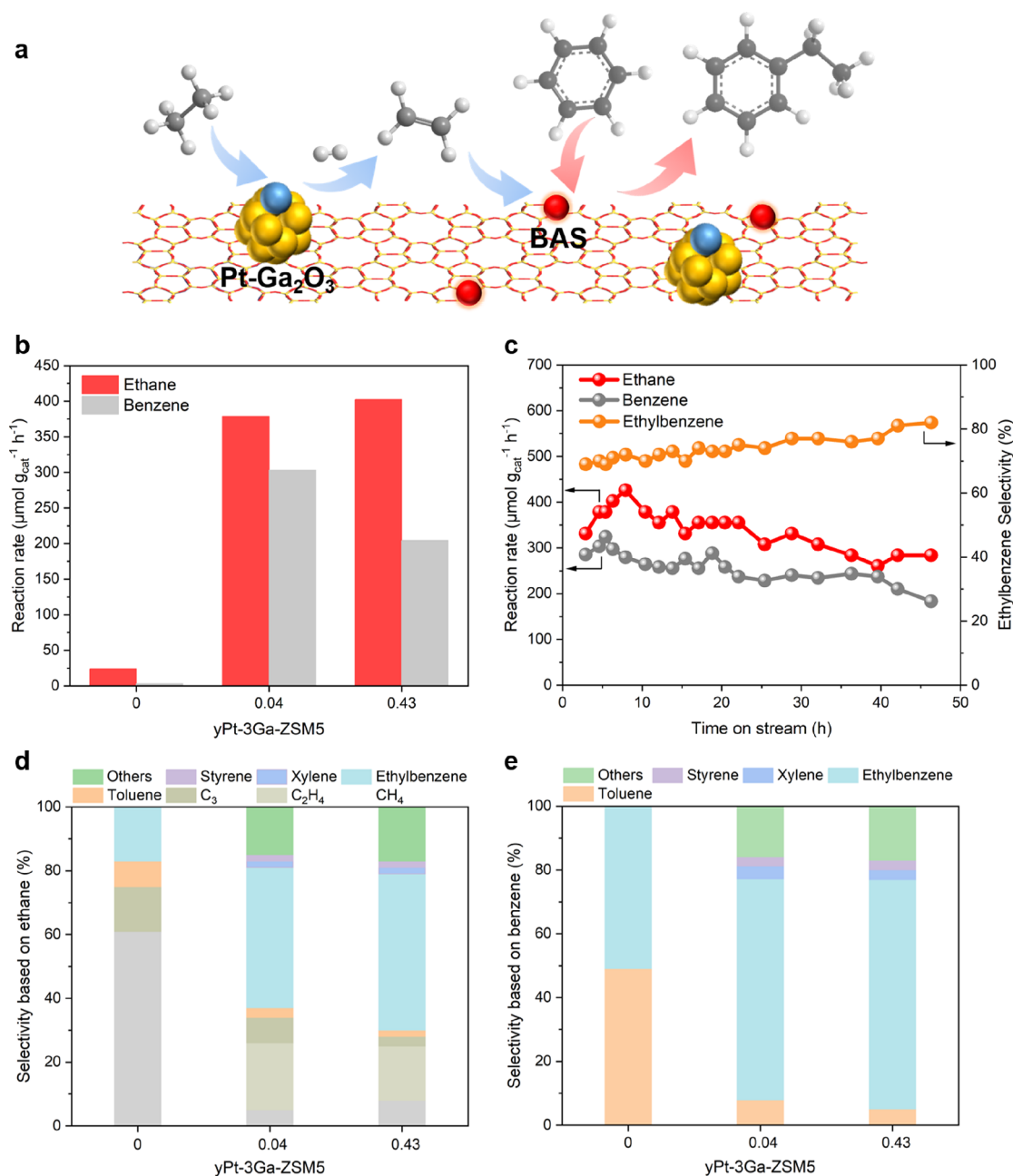
**Figure 7.** Catalytic performances for the ethane−benzene coupling reaction. (a) Schematic diagram of the reaction of ethane and benzene to ethylbenzene. (b) Conversion rates of ethane and benzene on different metal-zeolite catalysts. (c) Stability test of the 0.04Pt-3Ga-ZSM5 catalyst for the ethane−benzene coupling reaction. The reaction rates of ethane and benzene as well as the selectivity to ethylbenzene are displayed. (d) Product distribution of different metal-zeolite catalysts calculated based on ethane. (e) Product distribution of different metal-zeolite catalysts calculated based on benzene. Reaction conditions: 400 °C, a mixture of ethane and benzene (ethane/benzene molar ratio of 9) as the reaction feed, and weight hourly space velocity at 0.71 h$^{-1}$ based on ethane. The other products shown in panels (e−d) are mainly made by trimethylbenzene and other heavy aromatics.

0.43Pt-3Ga-ZSM5 sample, as implied by its lower activity for benzene conversion (Figure 7b). Previous work shows that the extra framework Pt species may prefer to be located around the Brønsted acid sites, which may partly neutralize the acidity.[41] In comparison with the reported materials for this reaction, the 0.04Pt-3Ga-ZSM5 sample gives the highest normalized activity to date, suggesting the high catalytic efficiency of atomically dispersed Pt sites on Ga$_2$O$_3$ nanoparticles for activation of light alkanes and the synergy of metal active sites and Brønsted acid sites confined in a zeolite matrix as a bifunctional catalyst (Table S10). The stability test with the 0.04Pt-3Ga-ZSM5

sample confirms its good stability for >45 h with a minor decrease in activity but a slight increase in selectivity to ethylbenzene.

At the current stage, the ethane−benzene coupling reaction catalyzed by the PtGa-ZSM5 catalyst cannot directly compete with the industrial ethylene−benzene alkylation process in terms of efficiency and techno-economy.[51,52] From a practical point of view, the PtGa-ZSM5 catalyst may have some advantages in the synthesis of long-chain alkylbenzene by the direct coupling of long-chain alkanes and benzene through a tandem dehydrogenation−alkylation process. For that purpose,

the porosity of the ZSM-5 zeolite needs to be adjusted for accommodation of the reactants and products, which are larger than those in the ethane−benzene coupling reaction.

## CONCLUSIONS

In this work, we have shown the generation of subnanometer bimetallic Pt-GaO$_x$ sites confined in ZSM-5 zeolite as active and stable sites for the activation of ethane. The bimetallic Pt-GaO$_x$ clusters follow different reaction mechanisms compared to the conventional bimetallic PtGa clusters, providing new insights into understanding the nature of the atomically dispersed metal catalysts supported on metal oxides or metal-zeolite supports for activation of light alkanes.[18,28] In particular, the particle size of the oxide support for hosting single metal atoms should also be carefully considered when designing the active sites based on bimetallic metal oxide clusters.

## ASSOCIATED CONTENT

### Supporting Information

The Supporting Information is available free of charge at https://pubs.acs.org/doi/10.1021/jacsau.4c00480.

> Experimental details, chemical compositions of the metal-zeolite materials, electron microscopy and spectroscopy results of the metal-zeolite materials, results of catalytic tests and theoretical calculations, characterizations of the spent catalysts, and summary of the catalytic performances reported in the literature works (PDF)

## AUTHOR INFORMATION

### Corresponding Authors

**Peng He** − State Key Laboratory of Coal Conversion, Institute of Coal Chemistry, Chinese Academy of Sciences, Taiyuan 030001, China; National Energy R&D Center for Coal to Liquid Fuels, Synfuels China Technology Co., Ltd., Beijing 101407, P. R. China; orcid.org/0000-0002-7141-4660; Email: hepeng@sxicc.ac.cn

**Liang Zhang** − Center for Combustion Energy and School of Vehicle and Mobility, Tsinghua University, Beijing 100084, China; orcid.org/0000-0002-9718-0436; Email: zhangbright@tsinghua.edu.cn

**Lichen Liu** − Engineering Research Center of Advanced Rare-Earth Materials of Ministry of Education, Department of Chemistry, Tsinghua University, Beijing 100084, China; orcid.org/0000-0001-5067-0481; Email: lichenliu@mail.tsinghua.edu.cn

### Authors

**Xiaomeng Dou** − Engineering Research Center of Advanced Rare-Earth Materials of Ministry of Education, Department of Chemistry, Tsinghua University, Beijing 100084, China

**Kailang Li** − Center for Combustion Energy and School of Vehicle and Mobility, Tsinghua University, Beijing 100084, China

**Kun Zhang** − State Key Laboratory of Coal Conversion, Institute of Coal Chemistry, Chinese Academy of Sciences, Taiyuan 030001, China; National Energy R&D Center for Coal to Liquid Fuels, Synfuels China Technology Co., Ltd., Beijing 101407, P. R. China; orcid.org/0009-0008-8713-8497

**Chaofeng Zhu** − Engineering Research Center of Advanced Rare-Earth Materials of Ministry of Education, Department of Chemistry, Tsinghua University, Beijing 100084, China

**Debora M. Meira** − CLS@APS Sector 20, Advanced Photon Source, Argonne National Laboratory, Argonne, Illinois 60439, United States; Canadian Light Source, Inc., Saskatoon, Saskatchewan S7N 2 V3, Canada; orcid.org/0000-0002-7529-2736

**Yang Song** − Center for Renewable Energy, Research Institute of Petroleum Processing, Beijing 100083, China; orcid.org/0000-0003-4212-8814

Complete contact information is available at:
https://pubs.acs.org/10.1021/jacsau.4c00480

### Author Contributions

◆X.D., K.L., and K.Z. contributed equally to this work. CRediT: **Kailang Li** data curation, investigation.

### Notes

The authors declare no competing financial interest.

## REFERENCES

(1) Li, X.; Pei, C.; Gong, J. Shale gas revolution: Catalytic conversion of C1−C3 light alkanes to value-added chemicals. *Chem.* **2021**, 7 (7), 1755−1801.

(2) del Campo, P.; Martínez, C.; Corma, A. Activation and conversion of alkanes in the confined space of zeolite-type materials. *Chem. Soc. Rev.* **2021**, 50 (15), 8511−8595.

(3) Xiang, Y.; Wang, H.; Cheng, J.; Matsubu, J. Progress and prospects in catalytic ethane aromatization. *Catal. Sci. Technol.* **2018**, 8 (6), 1500−1516.

(4) Ren, T.; Patel, M.; Blok, K. Olefins from conventional and heavy feedstocks: Energy use in steam cracking and alternative processes. *Energy* **2006**, 31 (4), 425−451.

(5) Yacob, S.; Caulfield, M.; Larson, R. B.; Gomez, E.; Meyer, R. J. The Interplay between Process Conceptualization and Experimental Research—Accelerating and Guiding Catalysis to Process Breakthroughs. *ACS Catal.* **2022**, 12 (17), 10621−10628.

(6) Saito, H.; Sekine, Y. Catalytic conversion of ethane to valuable products through non-oxidative dehydrogenation and dehydroaromatization. *RSC Adv.* **2020**, 10 (36), 21427−21453.

(7) Liu, L.; Corma, A. Isolated metal atoms and clusters for alkane activation: Translating knowledge from enzymatic and homogeneous to heterogeneous systems. *Chem.* **2021**, 7 (9), 2347−2384.

(8) Pan, Y.; Bhowmick, A.; Wu, W.; Zhang, Y.; Diao, Y.; Zheng, A.; Zhang, C.; Xie, R.; Liu, Z.; Meng, J.; et al. Titanium Silicalite-1

Nanosheet-Supported Platinum for Non-oxidative Ethane Dehydrogenation. *ACS Catal.* **2021**, *11* (15), 9970−9985.

(9) Galvita, V.; Siddiqi, G.; Sun, P.; Bell, A. T. Ethane dehydrogenation on Pt/Mg(Al)O and PtSn/Mg(Al)O catalysts. *J. Catal.* **2010**, *271* (2), 209−219.

(10) Wu, J.; Mallikarjun Sharada, S.; Ho, C.; Hauser, A. W.; Head-Gordon, M.; Bell, A. T. Ethane and propane dehydrogenation over PtIr/Mg(Al)O. *Appl. Catal. A: Gen.* **2015**, *506*, 25−32.

(11) Yu, Z.; Sawada, J. A.; An, W.; Kuznicki, S. M. PtZn-ETS-2: A novel catalyst for ethane dehydrogenation. *AIChE J.* **2015**, *61* (12), 4367−4376.

(12) Payard, P. A.; Rochlitz, L.; Searles, K.; Foppa, L.; Leuthold, B.; Safonova, O. V.; Comas-Vives, A.; Copéret, C. Dynamics and Site Isolation: Keys to High Propane Dehydrogenation Performance of Silica-Supported PtGa Nanoparticles. *JACS Au* **2021**, *1* (9), 1445−1458.

(13) Searles, K.; Chan, K. W.; Mendes Burak, J. A.; Zemlyanov, D.; Safonova, O.; Copéret, C. Highly Productive Propane Dehydrogenation Catalyst Using Silica-Supported Ga−Pt Nanoparticles Generated from Single-Sites. *J. Am. Chem. Soc.* **2018**, *140* (37), 11674−11679.

(14) Sun, G.; Zhao, Z. J.; Mu, R.; Zha, S.; Li, L.; Chen, S.; Zang, K.; Luo, J.; Li, Z.; Purdy, S. C.; Kropf, A. J.; Miller, J. T.; Zeng, L.; Gong, J. Breaking the scaling relationship via thermally stable Pt/Cu single atom alloys for catalytic dehydrogenation. *Nat. Commun.* **2018**, *9* (1), 4454.

(15) Chang, Q.-Y.; Wang, K.-Q.; Sui, Z.-J.; Zhou, X.-G.; Chen, D.; Yuan, W.-K.; Zhu, Y.-A. Rational Design of Single-Atom-Doped Ga2O3 Catalysts for Propane Dehydrogenation: Breaking through Volcano Plot by Lewis Acid−Base Interactions. *ACS Catal.* **2021**, *11* (9), 5135−5147.

(16) Sattler, J. J. H. B.; Gonzalez-Jimenez, I. D.; Luo, L.; Stears, B. A.; Malek, A.; Barton, D. G.; Kilos, B. A.; Kaminsky, M. P.; Verhoeven, T. W. G. M.; Koers, E. J.; et al. Platinum-Promoted Ga/Al2O3 as Highly Active, Selective, and Stable Catalyst for the Dehydrogenation of Propane. *Angew. Chem., Int. Ed.* **2014**, *53* (35), 9251−9256.

(17) Wang, P.; Yao, J.; Jiang, Q.; Gao, X.; Lin, D.; Yang, H.; Wu, L.; Tang, Y.; Tan, L. Stabilizing the isolated Pt sites on PtGa/Al2O3 catalyst via silica coating layers for propane dehydrogenation at low temperature. *Appl. Catal. B: Environ.* **2022**, *300*, No. 120731.

(18) Zhang, T.; Pei, C.; Sun, G.; Chen, S.; Zhao, Z. J.; Sun, S.; Lu, Z.; Xu, Y.; Gong, J. Synergistic Mechanism of Platinum-GaOx Catalysts for Propane Dehydrogenation. *Angew. Chem., Int. Ed.* **2022**, *61* (35), No. e202201453.

(19) Im, J.; Choi, M. Physicochemical Stabilization of Pt against Sintering for a Dehydrogenation Catalyst with High Activity, Selectivity, and Durability. *ACS Catal.* **2016**, *6* (5), 2819−2826.

(20) Liu, L.; Corma, A. Confining isolated atoms and clusters in crystalline porous materials for catalysis. *Nat. Rev. Mater.* **2021**, *6* (3), 244−263.

(21) Wang, H.; Wang, L.; Xiao, F.-S. Metal@Zeolite Hybrid Materials for Catalysis. *ACS Centr. Sci.* **2020**, *6* (10), 1685−1697.

(22) Chai, Y.; Shang, W.; Li, W.; Wu, G.; Dai, W.; Guan, N.; Li, L. Noble Metal Particles Confined in Zeolites: Synthesis, Characterization, and Applications. *Adv. Sci.* **2019**, *6* (16), No. 1900299.

(23) Zhang, Q.; Gao, S.; Yu, J. Metal Sites in Zeolites: Synthesis, Characterization, and Catalysis. *Chem. Rev.* **2023**, *123* (9), 6039−6106.

(24) Liu, L.; Lopez-Haro, M.; Lopes, C. W.; Li, C.; Concepcion, P.; Simonelli, L.; Calvino, J. J.; Corma, A. Regioselective generation and reactivity control of subnanometric platinum clusters in zeolites for high-temperature catalysis. *Nat. Mater.* **2019**, *18* (8), 866−873.

(25) Liu, L. C.; Lopez-Haro, M.; Lopes, C. W.; Rojas-Buzo, S.; Concepcion, P.; Manzorro, R.; Simonelli, L.; Sattler, A.; Serna, P.; Calvino, J. J.; et al. Structural modulation and direct measurement of subnanometric bimetallic PtSn clusters confined in zeolites. *Nat. Catal.* **2020**, *3* (8), 628−638.

(26) Sun, Q.; Wang, N.; Fan, Q.; Zeng, L.; Mayoral, A.; Miao, S.; Yang, R.; Jiang, Z.; Zhou, W.; Zhang, J.; et al. Subnanometer Bimetallic Platinum−Zinc Clusters in Zeolites for Propane Dehydrogenation. *Angew. Chem., Int. Ed.* **2020**, *132* (44), 19618−19627.

(27) Zhang, B.; Zheng, L.; Zhai, Z.; Li, G.; Liu, G. Subsurface-Regulated PtGa Nanoparticles Confined in Silicalite-1 for Propane Dehydrogenation. *ACS Appl. Mater. Interfaces* **2021**, *13* (14), 16259−16266.

(28) Dou, X.; Li, W.; Zhang, K.; Hou, H.; He, Z.; Zhu, C.; Meira, D. M.; Lopez-Haro, M.; Xia, Z.; He, P.; et al. Size-Dependent Structural Features of Subnanometer PtSn Catalysts Encapsulated in Zeolite for Alkane Dehydrogenation. *ACS Catal.* **2024**, *14* (5), 2859−2871.

(29) Yuan, Y.; Zhao, Z.; Lobo, R. F.; Xu, B. Site Diversity and Mechanism of Metal-Exchanged Zeolite Catalyzed Non-Oxidative Propane Dehydrogenation. *Adv. Sci.* **2023**, *10* (13), No. 2207756.

(30) Yuan, Y.; Lobo, R. F.; Xu, B. Ga2O22+ Stabilized by Paired Framework Al Atoms in MFI: A Highly Reactive Site in Nonoxidative Propane Dehydrogenation. *ACS Catal.* **2022**, *12* (3), 1775−1783.

(31) Yuan, Y.; Brady, C.; Lobo, R. F.; Xu, B. Understanding the Correlation between Ga Speciation and Propane Dehydrogenation Activity on Ga/H-ZSM-5 Catalysts. *ACS Catal.* **2021**, *11* (16), 10647−10659.

(32) Schreiber, M. W.; Plaisance, C. P.; Baumgärtl, M.; Reuter, K.; Jentys, A.; Bermejo-Deval, R.; Lercher, J. A. Lewis−Brønsted Acid Pairs in Ga/H-ZSM-5 To Catalyze Dehydrogenation of Light Alkanes. *J. Am. Chem. Soc.* **2018**, *140* (14), 4849−4859.

(33) Phadke, N. M.; Mansoor, E.; Bondil, M.; Head-Gordon, M.; Bell, A. T. Mechanism and Kinetics of Propane Dehydrogenation and Cracking over Ga/H-MFI Prepared via Vapor-Phase Exchange of H-MFI with GaCl3. *J. Am. Chem. Soc.* **2019**, *141* (4), 1614−1627.

(34) Sun, G.; Zhao, Z. J.; Li, L.; Pei, C.; Chang, X.; Chen, S.; Zhang, T.; Tian, K.; Sun, S.; Zheng, L.; Gong, J. Metastable gallium hydride mediates propane dehydrogenation on H2 co-feeding. *Nat. Chem.* **2024**, *11* (1), 575−583.

(35) Zhang, K.; Dou, X.; Hou, H.; Zhou, Z.; Lopez-Haro, M.; Meira, D. M.; Liu, P.; He, P.; Liu, L. Generation of Subnanometer Metal Clusters in Silicoaluminate Zeolites as Bifunctional Catalysts. *JACS Au* **2023**, *3* (11), 3213−3226.

(36) Liu, L.; Lopez-Haro, M.; Calvino, J. J.; Corma, A. Tutorial: structural characterization of isolated metal atoms and subnanometric metal clusters in zeolites. *Nat. Protoc.* **2021**, *16* (4), 1871−1906.

(37) Redekop, E. A.; Galvita, V. V.; Poelman, H.; Bliznuk, V.; Detavernier, C.; Marin, G. B. Delivering a Modifying Element to Metal Nanoparticles via Support: Pt−Ga Alloying during the Reduction of Pt/Mg(Al,Ga)Ox Catalysts and Its Effects on Propane Dehydrogenation. *ACS Catal.* **2014**, *4* (6), 1812−1824.

(38) Wan, H.; Qian, L.; Gong, N.; Hou, H.; Dou, X.; Zheng, L.; Zhang, L.; Liu, L. Size-Dependent Structures and Catalytic Properties of Supported Bimetallic PtSn Catalysts for Propane Dehydrogenation Reaction. *ACS Catal.* **2023**, *13* (11), 7383−7394.

(39) Kou, J.; Zhu Chen, J.; Gao, J.; Zhang, X.; Zhu, J.; Ghosh, A.; Liu, W.; Kropf, A. J.; Zemlyanov, D.; Ma, R.; et al. Structural and Catalytic Properties of Isolated Pt2+ Sites in Platinum Phosphide (PtP2). *ACS Catal.* **2021**, *11* (21), 13496−13509.

(40) Maurer, F.; Jelic, J.; Wang, J.; Gänzler, A.; Dolcet, P.; Wöll, C.; Wang, Y.; Studt, F.; Casapu, M.; Grunwaldt, J.-D. Tracking the formation, fate and consequence for catalytic activity of Pt single sites on CeO2. *Nat. Catal.* **2020**, *3* (10), 824−833.

(41) Felvey, N.; Guo, J.; Rana, R.; Xu, L.; Bare, S. R.; Gates, B. C.; Katz, A.; Kulkarni, A. R.; Runnebaum, R. C.; Kronawitter, C. X. Interconversion of Atomically Dispersed Platinum Cations and Platinum Clusters in Zeolite ZSM-5 and Formation of Platinum gem-Dicarbonyls. *J. Am. Chem. Soc.* **2022**, *144* (30), 13874−13887.

(42) Zhou, Y.; Thirumalai, H.; Smith, S. K.; Whitmire, K. H.; Liu, J.; Frenkel, A. I.; Grabow, L. C.; Rimer, J. D. Ethylene Dehydroaromatization over Ga-ZSM-5 Catalysts: Nature and Role of Gallium Speciation. *Angew. Chem., Int. Ed.* **2020**, *59* (44), 19592−19601.

(43) Liu, L.; Corma, A. Identification of the active sites in supported subnanometric metal catalysts. *Nat. Catal.* **2021**, *4* (6), 453−456.

(44) Finzel, J.; Sanroman Gutierrez, K. M.; Hoffman, A. S.; Resasco, J.; Christopher, P.; Bare, S. R. Limits of Detection for EXAFS Characterization of Heterogeneous Single-Atom Catalysts. *ACS Catal.* **2023**, *13* (9), 6462−6473.

(45) Huang, M.; Yasumura, S.; Li, L.; Toyao, T.; Maeno, Z.; Shimizu, K.-i. High-loading Ga-exchanged MFI zeolites as selective and coke-resistant catalysts for nonoxidative ethane dehydrogenation. *Catal. Sci. Technol.* **2022**, *12* (3), 986−995.

(46) Huang, M.; Maeno, Z.; Toyao, T.; Shimizu, K.-i. Ga speciation and ethane dehydrogenation catalysis of Ga-CHA and MOR: Comparative investigation with Ga-MFI. *Catal. Today* **2023**, *411−412*, No. 113824.

(47) Motagamwala, A. H.; Almallahi, R.; Wortman, J.; Igenegbai, V. O.; Linic, S. Stable and selective catalysts for propane dehydrogenation operating at thermodynamic limit. *Science* **2021**, *373* (6551), 217−222.

(48) Wang, T.; Radovanovic, P. V. Size-Dependent Electron Transfer and Trapping in Strongly Luminescent Colloidal Gallium Oxide Nanocrystals. *J. Phys. Chem. C* **2011**, *115* (38), 18473−18478.

(49) Wang, T.; Farvid, S. S.; Abulikemu, M.; Radovanovic, P. V. Size-Tunable Phosphorescence in Colloidal Metastable $\gamma$-Ga2O3 Nanocrystals. *J. Am. Chem. Soc.* **2010**, *132* (27), 9250−9252.

(50) Nakaya, Y.; Hirayama, J.; Yamazoe, S.; Shimizu, K. I.; Furukawa, S. Single-atom Pt in intermetallics as an ultrastable and selective catalyst for propane dehydrogenation. *Nat. Commun.* **2020**, *11* (1), 2838.

(51) Takabatake, M.; Hashimoto, A.; Chun, W.-J.; Nambo, M.; Manaka, Y.; Motokura, K. Dehydrogenative Coupling of Alkanes and Benzene Enhanced by Slurry-Phase Interparticle Hydrogen Transfer. *JACS Au* **2021**, *1* (2), 124−129.

(52) Misaki, S.; Ariga-Miwa, H.; Ito, T. U.; Yoshida, T.; Hasegawa, S.; Nakamura, Y.; Tokutake, S.; Takabatake, M.; Shimomura, K.; Chun, W.-J.; et al. Pd Nanoparticles on the Outer Surface of Microporous Aluminosilicates for the Direct Alkylation of Benzenes using Alkanes. *ACS Catal.* **2023**, *13* (18), 12281−12287.